Draft version October 10, 2016
Preprint typeset using LaTeX style emulateapj v. 5/2/11

THE LINEAR INSTABILITY OF DILUTE ULTRARELATIVISTIC $e^{\pm}$ PAIR BEAMS

Philip Chang[1], Avery E. Broderick[2,3], Christoph Pfrommer[4], Ewald Puchwein[5], Astrid Lamberts[6], Mohamad Shalaby[2,3,7], Geoffrey Vasil[8]

Draft version October 10, 2016

ABSTRACT

The annihilation of TeV photons from extragalactic TeV sources and the extragalactic background light produces ultrarelativistic $e^{\pm}$ beams, which are subject to powerful plasma instabilities that sap their kinetic energy. Here we study the linear phase of the plasma instabilities that these pair beams drive. To this end, we calculate the linear growth rate of the beam plasma and oblique instability in the electrostatic approximation in both the reactive and kinetic regimes, assuming a Maxwell-Jüttner distribution for the pair beam. We reproduce the well-known reactive and kinetic growth rates for both the beam plasma and oblique mode. We demonstrate for the oblique instability that there is a broad spectrum of unstable modes that grow at the maximum rate for a wide range of beam temperatures and wave vector orientations relative to the beam. We also delineate the conditions for applicability for the reactive and kinetic regimes and find that the beam plasma mode transitions to the reactive regime at a lower Lorentz factor than the oblique mode due to a combination of their different scalings and the anisotropy of the velocity dispersions. Applying these results to the ultrarelativistic $e^{\pm}$ beams from TeV blazars, we confirm that these beams are unstable to both, the kinetic oblique mode and the reactive beam-plasma mode. These results are important in understanding how powerful plasma instabilities may sap the energy of the ultrarelativistic $e^{\pm}$ beams as they propagate through intergalactic space.

Subject headings: BL Lacertae objects: general – gamma rays: general – plasmas – instabilities – magnetic fields

1. INTRODUCTION

The Fermi satellite and ground-based imaging atmospheric Cherenkov telescopes such as H.E.S.S., MAGIC, and VERITAS[9] have demonstrated that the high energy Universe is teeming with energetic very high-energy gamma-ray (VHEGR, $E > 100\,\mathrm{GeV}$) sources, the extragalactic component of which mainly consists of TeV blazars with a minority population of other sources such as radio and starburst galaxies. These extragalactic VHEGR emitters produce TeV photons that are greatly attenuated via annihilation upon soft photons in the extragalactic background light (EBL) and produce pairs (see, e.g., Gould & Schréder 1967a; Salamon & Stecker 1998; Neronov & Semikoz 2009).

It has been assumed that these ultrarelativistic pairs produced by VHEGR annihilation lose energy exclusively through inverse-Compton (IC) scattering off of the cosmic microwave background (CMB), transferring the energy of the original VHEGR to gamma-rays with energies $\lesssim 100\,\mathrm{GeV}$. The absence of observed secondary IC emission leads a number of authors to argue that this *lack* of emission places lower bounds upon the intergalactic magnetic field (IGMF; see, e.g., Neronov & Vovk 2010; Tavecchio et al. 2010, 2011; Dermer et al. 2011; Taylor et al. 2011; Takahashi et al. 2012; Dolag et al. 2011) with typical numbers ranging from $10^{-19}\,\mathrm{G}$ to $10^{-15}\,\mathrm{G}$.

In addition, Fermi has also provided the most precise estimate of the unresolved extragalactic gamma-ray background (EGRB) for energies between 200 MeV and 100 GeV. Since inverse-Compton cascades (ICCs) reprocess the VHEGR emission of distant sources into this band, this has been used to constrain the evolution of the luminosity density of VHEGR sources (see, e.g., Narumoto & Totani 2006; Kneiske & Mannheim 2008; Inoue & Totani 2009; Venters 2010). These constraints preclude any dramatic rise in numbers of source by $z \approx 1$–2 that is seen in the quasar distribution. That is, the comoving number of blazars must have remained essentially fixed, at odds with both the physical picture underlying these systems and with the observed evolution of similarly accreting systems, i.e., quasars and radio galaxies.

These two important conclusions depend on IC cooling dominating the evolution of the ultra-relativistic pairs. However, it was recently found that plasma instabilities driven by the ultrarelativistic pair beams likely are the dominant cooling mechanisms (Broderick et al. 2012, hereafter BCP12, Schlickeiser et al. 2012b, 2013), de-

[1] Department of Physics, University of Wisconsin-Milwaukee, 3135 North Maryland Avenue, Milwaukee, WI 53211, USA; chang65@uwm.edu
[2] Perimeter Institute for Theoretical Physics, 31 Caroline Street North, Waterloo, ON, N2L 2Y5, Canada
[3] Department of Physics and Astronomy, University of Waterloo, 200 University Avenue West, Waterloo, ON, N2L 3G1, Canada
[4] Heidelberg Institute for Theoretical Studies, Schloss-Wolfsbrunnenweg 35, D-69118 Heidelberg, Germany; christoph.pfrommer@h-its.org
[5] Institute of Astronomy and Kavli Institute for Cosmology, University of Cambridge, Madingley Road, Cambridge, CB3 0HA, UK
[6] TAPIR, Mailcode 350-17, California Institute of Technology, Pasadena, CA 91125, USA
[7] Department of Physics, Faculty of Science, Cairo University, Giza 12613, Egypt
[8] School of Mathematics & Statistics, University of Sydney, NSW 2006, Australia
[9] High Energy Stereoscopic System, Major Atmospheric Gamma Imaging Cerenkov Telescope, Very Energetic Radiation Imaging Telescope Array System.

positing this energy as heat in the intergalactic medium (Chang et al. 2012; Pfrommer et al. 2012). Therefore, the lack of an observed IC halo emission from TeV blazars does not imply the existence of the IGMF as previous groups have argued (BCP12;Schlickeiser et al. 2012b, 2013). We note that the effectiveness of these plasma instabilities is complicated by nonlinear effects, which we briefly discuss below.

The deposition of kinetic energy into the IGM via plasma instabilities produces excess heating, which over cosmological time, may resolve a variety of puzzles, including explaining anomalies in the statistics of the high-redshift Lyα forest (Puchwein et al. 2012; Lamberts et al. 2015) and potentially explaining a number of the X-ray properties of groups and clusters and anomalies in galaxy formation on the scale of dwarfs (Pfrommer et al. 2012; Lu et al. 2013). We have recently shown that *if* the IC halos are ignored, it is possible to quantitatively reproduce the redshift and flux distributions of nearby hard gamma-ray blazars and the extragalactic gamma-ray background spectrum above 3 GeV simultaneously with a unified model of AGN evolution (Broderick et al. 2014a,b). All of these empirical successes provide circumstantial evidence for the presence of virulent plasma beam instabilities.

These potential implications of blazar heating rely on an understanding of the linear and nonlinear physics of these plasma instabilities. Recent work in this area has been inconclusive. For instance, Miniati & Elyiv (2013) argued that these instabilities are physically irrelevant for the cooling of these pair beams because they would saturate at a very low level due to nonlinear Landau damping (NLD). However, Chang et al. (2014) performed a detailed calculation of NLD to show that these plasma processes remain dominant. In addition, Sironi & Giannios (2014) performed particle-in-cell simulations of these plasma processes and argued that these processes saturate at a very low level. It is unclear, however, if the conclusions of their work is applicable to the parameter regime of blazar heating.

Additional nonlinear effects may also be important. For instance, for sufficiently powerful blazers, the modulation instability may operate (Schlickeiser et al. 2012b; Chang et al. 2014; Menzler & Schlickeiser 2015), allowing for a rapid transfer of electrostatic wave energy into thermal energy. For less powerful blazars, the combination of NLD and quasilinear damping, i.e., beam plateauing, will also reduce the rate of damping compared to the linear rate, and alters the resulting IC spectra (Menzler & Schlickeiser 2015). Further study of these effects will help clarify these points.

While a full nonlinear study is required, we focus on the nature of the linear instability in this paper, clarifying its robustness and regimes of applicability. We begin by studying the distribution function of the $e^{\pm}$ pairs that are produced from VHEGR-EBL photon annihilation. We study the evolution of a distribution function under Lorentz transformations to develop an analytic understanding of how the perpendicular and parallel velocity dispersions transform under boosts. Using this understanding, we then develop a simple description of the distribution function of the beam, which we then use to calculate the unstable modes analytically in both the reactive (hydrodynamic) and kinetic regimes.

Here the reactive instability refers to the instability where the entire beam participates in the instability. In particular, all the beam particles are resonant with the unstable wave on a timescale longer than the growth time of the instability. The reactive instability is also referred to as the hydrodynamic instability since the instability can be derived from the fluid equations instead of kinetic theory. On the other hand, in the kinetic regime, only a fraction of the beam particles are resonant with the beam over a the growth time of the instability, which reduces the growth rate compared to the reactive instability for the same beam density and beam Lorentz factor. We recover the well-known results for the reactive regime for both the beam-plasma and oblique modes. We also derive the growth rate for these two instabilities in the kinetic regime and delineate the range of applicability for both the reactive and kinetic cases and apply these results for ultrarelativistic $e^{\pm}$ pair beams.

This paper is organized as follows. In Section 2, we describe the transformation properties of an ultrarelativistic $e^{\pm}$ beam in terms of its distribution function. We then calculate the various linear instabilities that this beam is subject to in section 3. In particular, we pay careful attention to both the reactive (or hydrodynamic) and kinetic regimes of the beam plasma and oblique instabilities and the transition between the two. Applying these results to TeV $e^{\pm}$ pair beams that arise from TeV photon pair production in Section 4, we demonstrate that despite the extraordinary coldness of the beam we are always in the kinetic regime for the oblique mode, but may be in the reactive regime for the beam plasma mode. However, for the relevant parameters, the growth rates calculated in either regime are similar. We close with a discussion of the implications of this work and application of these results for nonlinear theory in Section 5.

2. ULTRARELATIVISTIC PAIR BEAMS FROM VHEGRS

As stated in the Introduction, VHEGR photons pair produce on encountering EBL photons as they propagate throughout the universe (Gould & Schréder 1966), and this attenuation of VHEGR flux has been used as a probe of the EBL (Stecker et al. 1992; de Jager et al. 1994; Aharonian et al. 2006). The basic requirement of this process is that the energies of the VHEGR ($E_{\rm ph}$) and the EBL photon ($E_{\rm ebl}$) exceed the rest mass energy of the $e^{\pm}$ pair in the center of momentum (COM) frame, i.e., $2EE_{\rm ebl}(1-\cos\theta) \geq 4m_e^2c^4$, where θ is the relative angle of propagation in the lab frame. As a result, an $e^{\pm}$ pair can be produced with Lorentz factor$\gamma = \left(1 - v^2/c^2\right)^{-1/2} \approx E/2m_ec^2$, where v is the velocity of the pairs (Gould & Schréder 1967a). Here, we discuss the distribution function of the pair beam that emerges from this process.

2.1. *Distribution Function of the Pair Beam*

In the COM frame of the beam, we assume that the distribution function is isotropic, such that $f = f(E)$ is just a function of energy. This equilibrium energy distribution of a relativistic thermal plasma gas is

$$f \propto \exp\left(-\frac{E}{k_BT}\right), \tag{1}$$

where E and T are the dimensionless energy and temperature in terms of a particles rest mass. In the non-relativistic case, this reduces to the Maxwell-Boltzmann distribution, while the relativistic version is known as the Maxwell-Jüttner distribution (Jüttner 1911).

The relativistic Maxwellian distribution can be extended to a drifting (or boosted) distribution via an appropriate Lorentz transformation. The relationship between the energies of the lab (boosted) frame and the COM frame is

$$E_{\rm COM} = \gamma_b \left(E_{\rm L} - \beta_b p_{\rm L,\parallel} \right), \tag{2}$$

where $\gamma_b = \gamma(v_b) = \left(1 - v_b^2/c^2\right)$ is the Lorentz factor of the beam and v_b is the bulk velocity of the pair beam. Inserting this into (1), we find the Maxwell-Jüttner distribution (Jüttner 1911; Wright & Hadley 1975)

$$f = \frac{n_b m_e c^2}{4\pi\gamma_b k_B T_b K_2(m_e c^2/k_B T_b) m_e^3 c^3} \times \exp\left(-\frac{\gamma_b (E - \mathbf{v}_b \cdot \mathbf{p})}{k_B T_b} \right), \tag{3}$$

where K_2 is the 2nd order modified Bessel function and T_b is the comoving temperature of the beam.

The Maxwell-Jüttner distribution leads to an anisotropic velocity spread parallel and perpendicular to the beam's direction. In Appendix A, we estimate how the parallel and perpendicular velocity spreads scale. The relevant results are:

$$\frac{\Delta v_\perp^2}{c^2} \approx \frac{2 k_B T_b}{\gamma_b^2 m_e c^2} \quad \text{and} \quad \frac{\Delta v_\parallel^2}{c^2} \approx \frac{k_B T_b}{\gamma_b^4 m_e c^2}, \tag{4}$$

where T is measured in the COM frame of the beam. These simple scalings of the perpendicular velocity dispersion and parallel velocity dispersions can be understood as a results of time dilation between two frames that are boosted relative to each other, giving one factor of γ^{-1}. The coordinates perpendicular to the boost axis remain invariant while the axis along the boost suffers from length contraction and gives an extra scaling of γ^{-1} for the parallel case. In any case, an ultrarelativistic beam has a small velocity spread in both the parallel and perpendicular directions by factors of γ^{-2} and γ^{-1}, respectively. These velocity dispersions will be important in delineating the regime of instability in § 3.3.

While we have modeled the pair distribution function as a Maxwell-Jüttner distribution, the physical distribution function that is produced by VHEGR photo annihilation is somewhat more complicated (see for instance Schlickeiser et al. 2012a). In particular, the parallel and perpendicular momentum spread will be influenced by the distribution of VHEGR photons and their respective mean free paths. However, a Maxwell-Jüttner distribution is still useful. First, it also is sufficiently simple to allows us to calculate the kinetic instability exactly in the electrostatic approximation. Second, its instability growth rates has been calculated without approximation previously by Bret et al. (2010), allowing a point of comparison for our calculation using the electrostatic approximation (as mentioned below). Third, it possess a continuous (small) distribution of parallel and perpendicular momenta that allow us to elucidate the physics. Finally, the analytic methodology used to calculate the Maxwell-Jüttner distribution may be useful for the full calculation using the physical distribution function.

3. LINEAR THEORY

The Vlasov equation for each species is

$$\frac{\partial f_s}{\partial t} + \mathbf{v}_s \cdot \boldsymbol{\nabla} f_s + q_s \left(\mathbf{E} + \frac{\mathbf{v}_s}{c} \times \mathbf{B} \right) \cdot \boldsymbol{\nabla}_p f_s = 0, \tag{5}$$

where $\mathbf{v}_s = \mathbf{p}_s/\gamma_s m_e$ and $\gamma_s = 1/\sqrt{1 - v_s^2/c^2}$ Here, s is the species label, + for positrons and − for electrons, with $q_\pm = \pm e$. Upon linearizing this in small perturbations about a background distribution, i.e., setting $f_s \to f_{0s} + \delta f_s$, $\mathbf{B} \to \delta\mathbf{B}$ and $\mathbf{E} \to \delta\mathbf{E}$, we obtain,

$$\frac{\partial \delta f_s}{\partial t} + \mathbf{v}_s \cdot \boldsymbol{\nabla} \delta f_s + q_s \left(\delta\mathbf{E} + \frac{\mathbf{v}_s}{c} \times \delta\mathbf{B} \right) \cdot \boldsymbol{\nabla}_p f_{0s} = 0. \tag{6}$$

The plasma couples to the field through the Maxwell equations

$$\boldsymbol{\nabla} \times \delta\mathbf{E} = -\frac{1}{c} \frac{\partial \delta\mathbf{B}}{\partial t}, \tag{7}$$

$$\boldsymbol{\nabla} \times \delta\mathbf{B} = \frac{4\pi}{c} \delta\mathbf{j} + \frac{1}{c} \frac{\partial \delta\mathbf{E}}{\partial t}, \tag{8}$$

where $\delta\mathbf{j} = \sum_s q_s \int \mathbf{v} \delta f_s d^3p$ is the linear current density perturbation.

Here it is useful to work within the electrostatic approximation ($\mathbf{k} \times \delta\mathbf{E} = 0$), where we only need to include Coulomb's law for the electric field rather than the full Maxwell equations:

$$i\mathbf{k} \cdot \delta\mathbf{E} = 4\pi\delta\rho, \tag{9}$$

where $\delta\rho = \sum_s q_s \int \delta f_s \, d^3p$ is the perturbed charge density. By adopting the electrostatic approximation, we have explicitly ignored electromagnetic modes. This would preclude, for example, the Weibel instability. In addition, the electromagnetic terms would introduce corrections to the physics that are not necessarily small in the limit of relativistic particles, i.e., $v/c \to 1$. However, we make this approximation for two reasons. First, a complete calculation of the unstable modes has already been carried out by Bret et al. (2010), who showed that the oblique mode is mainly electrostatic (modulo the Weibel instability). Hence a electrostatic approximation to the full dispersion relation should recover the essential physics. Second, the electrostatic approximation is much simpler than a full calculation and allows us to analytically calculate the unstable growth rates, while permitting a clear exposition of the relevant physics.

We now adopt perturbations of the form $\delta \propto \exp\left(i\mathbf{k} \cdot \mathbf{r} - i\omega t\right)$ and without loss of generality assume that $\mathbf{k} = (k_x, 0, k_z)$, where k_z is along the beam direction. Linearizing the Vlasov-Maxwell equations then leads to the dispersion relation:

$$\epsilon = 1 + \sum_s \frac{m_e \omega_{p,s}^2}{k^2} \int \frac{\mathbf{k} \cdot \boldsymbol{\nabla}_p F_s}{\omega - \mathbf{k} \cdot \mathbf{v}} d^3p = 0, \tag{10}$$

where ϵ is the simplified dielectric function, and for each species $\omega_{p,s}^2 \equiv 4\pi e^2 n_s/m_e$ is the plasma frequency, $n_s \equiv \int f_{0s} d^3p$ is the number density, and $F_s \equiv f_{0s}/n_s$ is the normalized background distribution function. Upon

integrating by parts, Equation (10) becomes

$$\epsilon = 1 - \sum_s \frac{m_e \omega_{p,s}^2}{k^2} \int F_s \mathbf{k}\cdot\boldsymbol{\nabla}_p \frac{1}{\omega - \mathbf{k}\cdot\mathbf{v}} d^3p$$
$$= 1 - \sum_s \frac{\omega_{p,s}^2}{k^2 c^2} \int F_s \frac{k^2c^2 - (\mathbf{k}\cdot\mathbf{v})^2}{\gamma(\omega - \mathbf{k}\cdot\mathbf{v})^2} d^3p = 0\,. \quad (11)$$

There are two distinct, often qualitatively different, regimes in which we may consider the implications of this dispersion relation. The first is the cold plasma limit or the hydrodynamic or reactive limit. The hydrodynamic limit is aptly named because the resulting dispersion relation that is found could have also been calculated directly from the continuity equation and the momentum equation. In this limit, the internal distribution of the particles of the background or beam are irrelevant to the physics of the instability and it is only the bulk response that is important. In particular, this means that the beam particles are resonant with the unstable wave over a timescale much longer than the growth time, i.e., the beam particles do not drift a distance larger than the wavelength of the unstable mode over the growth time of the instability. The second is the kinetic regime, where the internal distribution of beam particles is important to the physics of the instability. Here, only a fraction of beam particles stay within one wavelength of the unstable mode over the growth time of the instability. Moreover, the bulk of the plasma (background or beam) does not respond to the disturbance; instead, only a fraction of particles is relevant for driving (instability) or damping (Landau damping). We discuss below the evaluation of the dispersion relation in these two regimes, which gives two regimes of instability, and the delineation between them.

3.1. *Hydrodynamic (Reactive) Instability*

Starting with the dispersion relation (11), we first consider the instability of a cold plasma beam. Taking the limit of Equation (3) as $k_B T_t \to 0$, for a target plasma $v_0 = 0$ and a beam plasma $v_0 = v_b$[10], we find

$$1 - \frac{\omega_{p,t}^2}{\omega^2} - \frac{\omega_{p,b}^2}{\gamma^3(\omega - k_z v_b)^2} \frac{\gamma^2 k_x^2 + k_z^2}{k_x^2 + k_z^2} = 0. \quad (12)$$

For $k_x = 0$, we recover the same beam-plasma instability which was described in the Appendix of BCP12.

The solution to Equation (12) is given in Appendix B where we show that the associated growth rate (Equation B6) is

$$\Gamma = \frac{\sqrt{3}}{2^{4/3}} \left(\frac{n_b}{n_t}\right)^{1/3} \left(\frac{\gamma^2 Z_x^2 + 1}{Z_x^2 + 1}\right)^{1/3} \frac{\omega_{p,t}}{\gamma}, \quad (13)$$

where $Z_x = k_x v_b/\omega_{p,t}$ is the dimensionless wavevector perpendicular to the beam direction.

For $k_x = 0 \to Z_x = 0$, this reduces to the beam-plasma growth rate, which is

$$\Gamma = \Gamma_{\rm TS} \equiv \frac{\sqrt{3}}{2^{4/3}} \left(\frac{n_b}{n_t}\right)^{1/3} \frac{\omega_{p,t}}{\gamma}, \quad (14)$$

which we denote the beam-plasma or "two-stream" growth rate. For the more general case where $Z_x \neq 0$, this becomes the oblique instability studied by Bret et al. (2010) Indeed for $\gamma \gg 1$ and $Z_x \gg 1$, the growth rate approaches the oblique growth rate:

$$\Gamma = \Gamma_{\rm ob} \equiv \frac{\sqrt{3}}{2^{4/3}} \left(\frac{n_b}{n_t}\right)^{1/3} \frac{\omega_{p,t}}{\gamma^{1/3}}, \quad (15)$$

which is much faster than the beam-plasma growth rate, $\Gamma_{\rm TS}$

We should caution in the derivation above that the resonance condition, which is $\omega_{p,t} - k_z v_b$, implies that $k_z \neq 0$. For the case where $k_z \to 0$, the electrostatic approximation no longer holds and the full dispersion relation must be solved.[11] A solution to the full dispersion relation reveals additional modes, including the zero frequency ($k_z = 0$) filamentation or Weibel mode.

Equation (12) can also be solved numerically in terms of k_x and k_z. Here let us specialize to the case of $k_x = 0$, i.e., the beam-plasma case. In this case, we have

$$1 - \frac{\omega_{p,t}^2}{\omega^2} - \frac{\omega_{p,b}^2}{\gamma^3(\omega - k_z v_b)^2} = 0, \quad (16)$$

which we can numerically solve in terms of $\omega/\omega_{p,t}$, $k_z\lambda_D$, v_b/c, and n_b/n_t, where $\lambda_D = c/\omega_{p,t}$ is the skin depth. In Figure 1 we show the real and imaginary parts for $\omega/\omega_{p,t}$ as a function of $k_z\lambda_D$ for the representative case of $v_b/c \approx 1$ and $n_b/n_t = 10^{-3}$ and $\gamma = 100$. For $k_z\lambda_D = 1$, the growth rate reaches it maximum of $\Gamma_{\rm max}$ and the real part of the frequency is $\Re(\omega) = \omega_{p,t}$, which is the plasma oscillation frequency. This wave would exist in the absence of a tenuous beam. However, as we move away from this frequency toward lower k_z, we still find substantial growth, with $\Gamma \approx 0.1\Gamma_{\rm max}$ as $k_z \approx 0.9\lambda_D^{-1}$. Interestingly, the real part of the unstable wave has a phase velocity, $v_{\rm ph} = \Re(\omega)/k = c$, which is still in resonance with the beam.

In a continuous system, these waves do not matter in comparison to the unstable mode at $k\lambda_D = 1$. However, for discrete numerical systems, which do not sufficiently resolve the most unstable modes, these submaximal modes drive the growth of the instability of numerically calculated beam-plasma systems, which may lead to an incorrect nonlinear state in comparison to the physical system.

3.2. *Kinetic Instability*

The growth rate expressed in Equation (13) is in the reactive (or hydrodynamic) regime as the dispersion relation (Equation 12) could have been derived from the fluid equations. Here all the particles participate in the instability. However, kinetic theory marks another regime of the instability, where only a fraction of the particle participate in the instability, i.e., the kinetic regime. We now derive the growth rate of the instability in the kinetic regime.

We begin first with the distribution function for the target plasma:

$$F_t = \left(\frac{1}{2\pi m_e k_B T_t}\right)^{3/2} \exp\left(-\frac{p^2}{2m_e k_B T_t}\right), \quad (17)$$

[10] That is, we set $F_s(\mathbf{p}) = \delta^3(\mathbf{p} - \mathbf{p}_{0s})$ where $\mathbf{p}_{0s} \equiv \gamma_0 m_e v_0 \hat{\mathbf{z}}$ is the momentum associated with v_0.

[11] We thank Antoine Bret for helping to clarify this point.

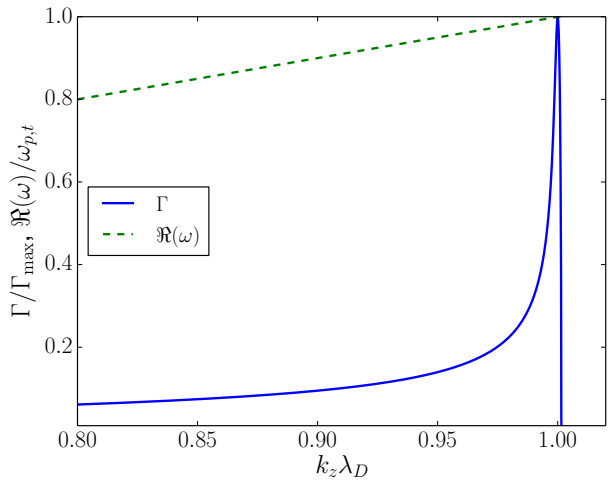

Figure 1. Beam-plasma growth rate (solid line) and unstable wave frequency (dashed-line) as a function of k_z for $\gamma_b = 100$ and $n_b/n_t = 10^{-3}$.

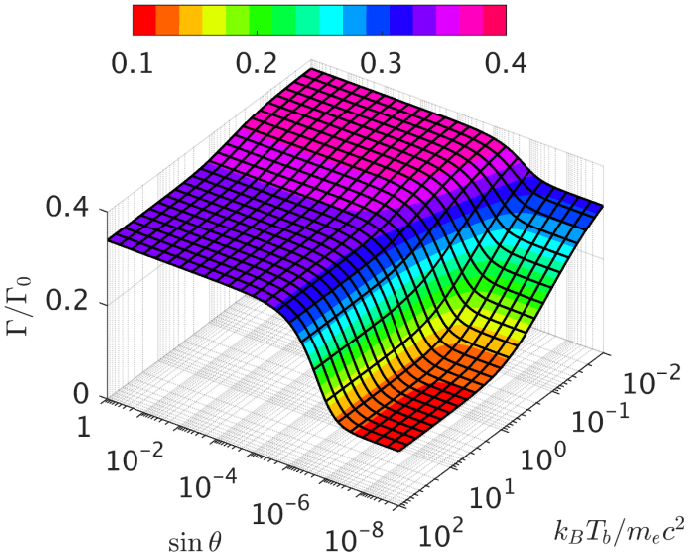

Figure 2. Oblique growth rate maximized over $v_{\rm ph}$ as a function of $\sin\theta$ and k_BT_b/m_ec^2, where θ is the angle between the beam direction and wavevector for $\gamma_b = 10^6$. The maximum growth rate occurs when $\sin\theta \gg 1/\gamma_b$. Note that as $\sin\theta \to 0$, we asymptote to the beam-plasma growth rate.

where the target plasma is assumed to be nonrelativistic, $\mathbf{p} = m_e\mathbf{v}$ is the nonrelativistic momentum, and T_t is the temperature of the target background plasma. For the beam plasma, we again adopt the Maxwell-Jüttner distribution (Equation 3). Inserting these into the dispersion relation (Equation 10), we find

$$1 - \frac{\omega_{p,t}^2}{k^2c^2}\int F_t \frac{k^2c^2 - (\mathbf{k}\cdot\mathbf{v})^2}{\gamma(\omega - \mathbf{k}\cdot\mathbf{v})^2} d^3p + \frac{m_e\omega_{p,b}^2}{k^2}\int \frac{\mathbf{k}\cdot\boldsymbol{\nabla}_p F_b}{\omega - \mathbf{k}\cdot\mathbf{v}} d^3p = 0, \tag{18}$$

where we have integrated by parts only the second term, associated with the target plasma.

We discuss the solution to Equation (18) in Appendix C. The associate growth rate for the kinetic oblique instability is

$$\Gamma \approx -\Gamma_0 \frac{\pi\gamma_w^2\gamma_{\rm ph}^3(v_{\rm ph} - v_{b,z'})}{4\gamma_b\mu^2K_2(\mu)\mathcal{G}'^3c} \times \left[\left(\mathcal{G}'^2\mu^2 + 2\mathcal{G}'\mu + 2\right) + \frac{\gamma_b^2 v_{b,x'}^2}{2\mathcal{G}'^2c^2}\left(2\mathcal{G}'\mu + 2\right)\right]\exp(-\mathcal{G}'\mu), \tag{19}$$

where $\mu = m_ec^2/k_BT_b$, $\gamma_{\rm ph} = \left(1 - v_{\rm ph}^2/c^2\right)^{-1/2}$, $v_{\rm ph} = \omega/k$ is the phase velocity of the wave, $v_{b,z'}$ is the velocity of the beam oriented along the wavevector, $v_{b,x'}$ is the velocity of the beam perpendicular to the wavevector, $\gamma_w = \left(1 - w^2/c^2\right)^{-1/2}$, $w = \gamma_{\rm ph}^{-1}v_{b,x'}/(1 - v_{b,z'}v_{\rm ph}/c^2)$ is the beam velocity transverse to the wavevector in a frame that is comoving with the wave at its phase velocity, and $\mathcal{G}' \equiv \gamma_b\gamma_{\rm ph}(1 - v_{b,z'}v_{\rm ph}/c^2)/\gamma_w$ is the Lorentz factor of a beam particle in a frame that is comoving with the wave at the phase velocity and the transverse (to the wavevector) beam bulk velocity Finally, we define the typical maximum growth rate, Γ_0, as

$$\Gamma_0 \equiv \omega_p\gamma_b\frac{n_b}{n_t}\frac{m_ev_b^2}{k_BT_b}. \tag{20}$$

Equation (19) specializes to the beam-plasma growth rate if we take $v_{b,x'} = 0$, which gives:

$$\Gamma_{\rm bp} \approx -\Gamma_0\frac{\pi\gamma_{\rm ph}^3(v_{\rm ph} - v_{b,z'})}{4\gamma_b\mu^2K_2(\mu)\mathcal{G}^3c}\left(\mathcal{G}^2\mu^2 + 2\mathcal{G}\mu + 2\right)\exp(-\mathcal{G}\mu), \tag{21}$$

where we have used the fact that $\gamma_w = 1$ for $v_{b,x'} = 0$

In Figure 2, we plot the growth rate for the oblique instability (Equation (19)) as a function of $\sin\theta$, where $\cos\theta = \hat{\mathbf{k}}\cdot\hat{\mathbf{v}}$, i.e., the angle between the beam and the wavevector, and k_BT_b/m_ec^2. Here, it is clear that the growth rate reaches its maximum value $\sin\theta \gtrsim 1/\gamma_b$, i.e., at an oblique angle. Note that as $\sin\theta \to 0$, we recover the beam-plasma instability. Moreover, the maximal growth rates, normalized to Γ_0, vary little and are robust for a broad range of angles between the wavevector and the beam direction. It is clear from this plot that for nearly any combination of wavevector orientation and beam temperature that there exists a broad spectrum of modes that are unstable and grow at nearly the maximum growth rate, Γ_0, for the parameters of the system, T_b, γ_b, and n_b/n_t, modulo a factor of order unity.

This does not imply that any individual mode, i.e., a mode with a fixed wavevector, will grow robustly. Any individual mode only grows when the phase velcocity of the mode in the direction of the beam are in resonance and this resonant width is narrow. However, the growth is robust as for any combination of wavevector orientation and beam temperature, there exists some mode that will grow at the maximum rate.

Because there is little variation in the maximal oblique growth rate as a wavevector orientation, we plot the maximum growth rate as a function of T_b and $\gamma_b - 1$ in Figure 3. Here for relativistic beams, the maximum growth rate varies little with T_b, varying by less than 10% between

hot and cold beams and we find:

$$\Gamma_M \approx \begin{cases} 0.38\Gamma_0 & k_B T_b/m_e c^2 \ll 1 \\ 0.34\Gamma_0 & k_B T_b/m_e c^2 \gg 1 \end{cases}, \quad (22)$$

for $\gamma_b \gtrsim 10$, as seen in Figure 3. Hence, unstable modes exists and robustly grow at roughly $\Gamma \approx 0.4\Gamma_0$ for nearly any value of $k_B T_b/m_e c^2$, wavevector orientation, and $\gamma_b \gg 1$.

This can be contrasted with the right panel of Figure 3 where we plot the beam-plasma growth rate (21) as a function of $\gamma_b - 1$ and $k_B T_b/m_e c^2$. Here, we see that the maximum growth rate is somewhat more sensitive to temperature, varying from $\Gamma/\Gamma_0 \approx 0.4$ for $k_B T_b/m_e c^2 \ll 1$ to $\Gamma/\Gamma_0 \approx 0.1$ for $k_B T_b/m_e c^2 \gtrsim 1$. Note, however, that that beam-plasma growth rate remains competitive with the oblique growth rate, i.e., it is not orders of magnitude lower.

Finally, the maximum growth rate that we derived here (Equation (22)) and that of BCP12 (their equation (16)) which is originally derived from the numerical fit of Bret et al. (2010) are exactly the same. We must note, however, that the our definition of T_b is in the COM frame whereas BCP12 defines T_b in the "lab" frame. As a result, there is a factor of γ_b that is explicit in Equation (22) that is implicit in Equation (16) of BCP12.

3.3. *The Transition between the Kinetic and Hydrodynamic Instability*

The oblique instability exists in two different regimes, raising the important question: how are the two regimes related to each other. While this question has been studied by many authors in the context of the beam-plasma or two-stream instability (see for instance Melrose 1986; Boyd & Sanderson 2003), a clear exposition of how these two regimes are related to each other for the oblique instability is lacking.

To begin let us return to the reactive instability. For the growth rate of the reactive instability in Equation (13) to be valid, the velocity dispersion must be vanishingly small. In particular, over the growth time of the unstable wave, the beam particles may not be spread significantly, i.e., their spread is much smaller than one wavelength. Quantitatively, this demands

$$\left| \frac{\mathbf{k} \cdot \Delta\mathbf{v}}{\Gamma} \right| \ll 1. \quad (23)$$

For $k_\perp \approx \omega_p/v_b$, this gives

$$\frac{\Delta v_\perp}{v_b} \ll \left(\frac{n_b}{\gamma_b n_t} \right)^{1/3} \quad (24)$$

where we have dropped constant factors of order unity and assumed that $Z_x \propto O(1)$ and that the velocity dispersion is dominated by perpendicular (to the beam) component. Hence, this defines the upper limit on the velocity dispersion of the plasma for the cold-plasma approximation to hold and, hence, the range of validity for the reactive oblique growth rate Equation (13). For $Z_x \ll \gamma^{-2}$, we recover the condition for the relativistic, reactive beam-plasma instability:

$$\frac{\Delta v_\parallel}{v_b} \ll \gamma_b^{-1} \left(\frac{n_b}{n_t} \right)^{1/3}. \quad (25)$$

Applying the scaling of the perpendicular and parallel velocity dispersions (Equations 4) to these results and assuming $v_b \approx c$, we find

$$\frac{\Delta v_\perp}{v_b} \approx \gamma_b^{-1} \sqrt{\frac{k_B T_b}{m_e c^2}} \quad \text{and} \quad \frac{\Delta v_\parallel}{v_b} \approx \gamma_b^{-2} \sqrt{\frac{k_B T_b}{m_e c^2}}. \quad (26)$$

Hence, the conditions for the reactive regime for the oblique mode (Equation 24) and beam-plasma mode (Equation 25) can be reduced to

$$1 \ll \begin{cases} (k_B T_b/m_e c^2)^{-1/2} \gamma_b^{2/3} (n_b/n_t)^{1/3} & \text{oblique} \\ (k_B T_b/m_e c^2)^{-1/2} \gamma_b (n_b/n_t)^{1/3} & \text{beam plasma} \end{cases}. \quad (27)$$

We now proceed to study the range of validity for the kinetic growth rate for the beam plasma mode (Equation 21) and oblique mode (Equation 19). Following the argument of Boyd & Sanderson (2003), the growth occurs over a range where the distribution function is positive or $v_b - \Delta v < \omega/k < v_b$. Hence the bandwidth over which the distribution powers grows is $\Delta\omega \approx k\Delta v$. For the kinetic growth rate to be valid, the bandwidth, $\Delta\omega$, must be large compared to the growth rate; otherwise, the entire beam contributes to the growth and, hence, the reactive regime applies. For the beam plasma case, the growth rate is roughly

$$\Gamma \approx \frac{n_b}{\gamma^3 n_t} \left(\frac{c}{\Delta v_\parallel} \right)^2. \quad (28)$$

The bandwidth, $\Delta\omega$, is then greater than the growth rate if

$$\frac{\Delta v_\parallel}{v_b} \gtrsim \gamma^{-1} \left(\frac{n_b}{n_t} \right)^{1/3}, \quad (29)$$

which connects with the condition on the reactive beam plasma instability from Equation (25). Similarly for the oblique mode, the bandwidth, $\Delta\omega$, is then greater than the growth rate if

$$\frac{\Delta v_\perp}{v_b} \gtrsim \left(\frac{n_b}{\gamma n_t} \right)^{1/3}, \quad (30)$$

which can similarly compared to the condition on the reactive oblique mode from Equation (24).

Combining these two kinetic condition and our result again from Section 2, we find

$$1 \geq \begin{cases} (k_B T_b/m_e c^2)^{-1/2} \gamma_b^{2/3} (n_b/n_t)^{1/3} & \text{oblique} \\ (k_B T_b/m_e c^2)^{-1/2} \gamma_b (n_b/n_t)^{1/3} & \text{beam plasma} \end{cases}, \quad (31)$$

which in combination with Equation (27) denotes the transition between the reactive and kinetic regimes.

4. APPLICATION TO ULTRARELATIVISTIC $e^\pm$ BEAMS

As discussed in the Introduction, the annihilation of VHEGRs and EBL photons produce ultrarelativistic $e^\pm$ beams that are unstable to the beam plasma and oblique modes discussed above. To apply the above results to the ultrarelativistic $e^\pm$ beams, we now calculate their initial conditions.

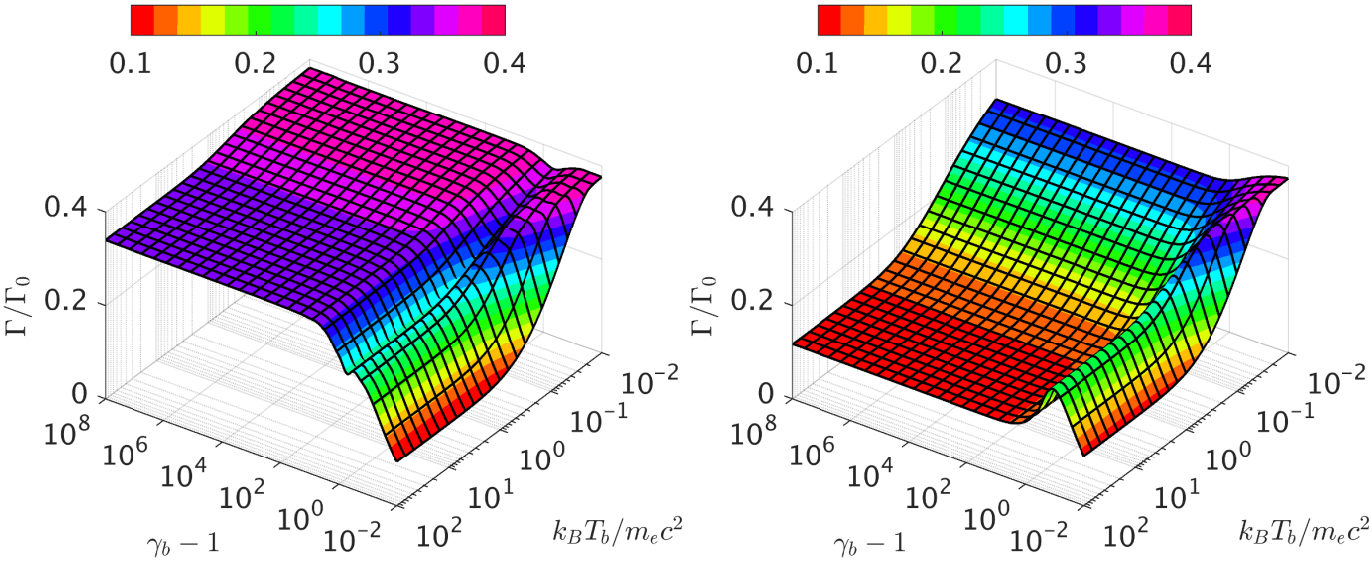

Figure 3. Oblique kinetic growth rate (left) and beam-plasma growth rate (right), and normalized by $\Gamma_0 \equiv \omega_{Pt}(n_b/n_t)\gamma_b m v_b^2/k_B T_b$ as a function of $k_B T_b/m_e c^2$ and $\gamma_b - 1$. The oblique kinetic growth rate has been maximized over θ. Unlike the beam-plasma case on the right, in the case of the oblique kinetic growth rate at high γ_b the transition between high and low temperature is only marginal, constituting a roughly 10% reduction.

4.1. *Average COM Energy of the $e^{\pm}$ Beam*

To find the effective velocity dispersion of the ultra-relativistic $e^{\pm}$ beam, we must first estimate the average COM energy of the beam. To do so, we consider the process of photon-photon annihilation. For a monoenergetic population of VHEGR photons with energy $E_{\rm ph}$, the angle-averaged production rate of $e^{\pm}$ on EBL photons is

$$\begin{aligned}\Gamma_{\pm}(E_{\rm ph}) &= \frac{1}{4\pi}\int \sigma c dn_{\rm EBL} d\Omega \\ &= \frac{1}{2}\int \sigma\left(E_{\rm ph}, E_{\rm EBL}, \theta\right) c \frac{dn_{\rm EBL}}{dE_{\rm EBL}} \\ &\quad dE_{\rm EBL} d\cos\theta,\end{aligned} \tag{32}$$

where $\Gamma_{\pm}$ is the rate of pair production, σ is the pair-production cross section, $n_{\rm EBL}$ is the number density of EBL photons, $E_{\rm EBL}$ is the energy of the EBL photons, and θ is the angle between the momentum of the VHEGR photon and the EBL photon. There are two important components to this calculation – the cross section, σ, and the spectrum of the EBL.

For σ, we use the results from Nikishov (1962) and Gould & Schréder (1967b), who considered a high energy photon with energy $E_{\rm ph}$ moving along the x-axis annihilating on an EBL photon with energy $E_{\rm EBL}$ moving at an angle, θ, with respect to the x-axis. The total cross section for this process is (Nikishov 1962; Gould & Schréder 1967b)

$$\begin{aligned}\sigma = \frac{1}{2}\pi r_e^2\left(1-\frac{v_e^2}{c^2}\right)\Bigg[\left(3-(v_e/c)^4\right)\ln\frac{1+v_e/c}{1-v_e/c} \\ -2\frac{v_e}{c}\left(2-\frac{v_e^2}{c^2}\right)\Bigg],\end{aligned} \tag{33}$$

where $r_e = e^2/m_e c^2$ is the classical electron radius and v_e is the electron velocity in the COM frame of the generated pair.[12] To find v_e, we use the energy of the electron in the COM frame, $E_{\rm e,COM}$, which is

$$E_{\rm e,COM} = \frac{m_e c^2}{\sqrt{1-v_e^2/c^2}} = \sqrt{\frac{1}{2}E_{\rm EBL}E_{\rm ph}\left(1-\cos\theta\right)}. \tag{34}$$

Pair production occurs when $E_{\rm e,COM}/m_e c^2 \geq 1$.

The second ingredient is the spectrum of the EBL, which is not well constrained. Here we use the constraints from Aharonian et al. (2006), who demonstrated that VHEGR emission from H 2356-309 and 1ES 1101-232 places an upper limit on the EBL that is close to the lower limit of the integrated light from galaxies Madau & Pozzetti (2000). Looking at Figure 1 of Aharonian et al. (2006), we note that the EBL has a flat spectrum, i.e., constant $dn_{\rm EBL}/dE_{\rm EBL}$ below 1 eV and a falling spectrum $dn_{\rm EBL}/dE_{\rm EBL} \propto E_{\rm EBL}^{-1.5}$ with a spectral index of ≈ 1.5 above 1 eV with a rapid cutoff above 10 eV. Thus, we adopt a simplified model:

$$\frac{dn_{\rm EBL}}{dE_{\rm EBL}} \propto \begin{cases} E_{\rm EBL}^{0} & E_{\rm EBL} \leq 1\,{\rm eV} \\ E_{\rm EBL}^{-1.5} & 1\,{\rm eV} < E_{\rm EBL} \leq 10\,{\rm eV} \\ 0 & E_{\rm EBL} > 10\,{\rm eV}. \end{cases} \tag{35}$$

In Figure 4, we plot the differential rate of pair production as a function of the COM energy of the electron (and positron), $E_{\rm e,COM}$ for a photon energy of $E_{\rm ph} = 0.3$ (dotted line), 1 (solid line), 3 (dash-dotted line) and 10 TeV (dashed line). Note the distribution of COM energy for the electrons (and positrons) depends on the initial photon energy. This is because different energy photons probe different regimes of the EBL spectrum. Due to the rapid cutoff in the EBL above 10 eV, lower energy VHEGRs produce colder beams. This is seen

[12] In this section, the COM frame and subscript "COM" refer to the center of momentum frame of the pair that is produced by a single $\gamma - \gamma$ annihilation.

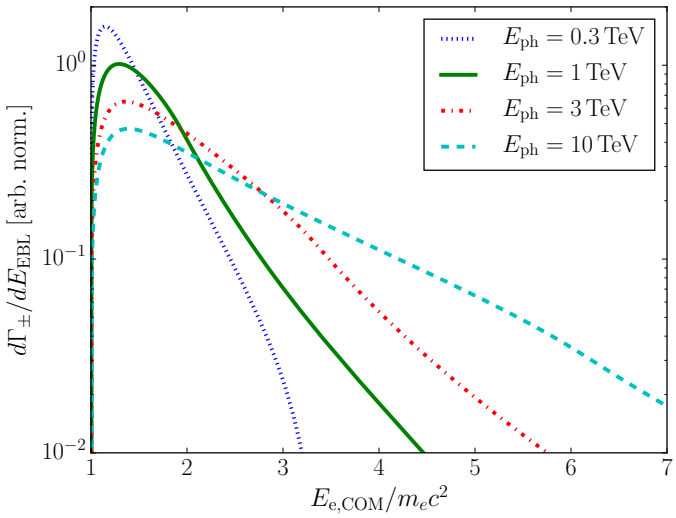

Figure 4. Differential rate of pair production as a function of the COM energy of the electron (and positron) for a photon energy of $E_{\rm ph} = 0.3$ (dotted line), 1 (solid line), 3 (dash-dotted line) and 10 TeV (dashed line). The effect of the EBL spectrum can be seen in different features in this plot. The cutoff in $d\Gamma_\pm/dE_{\rm EBL}$ above $E_{\rm e,COM}/m_ec^2 \approx 3$ for $E_{\rm ph} = 1\,{\rm TeV}$ is due to the cutoff in the EBL spectrum above 10 eV. The break in $d\Gamma_\pm/dE_{\rm EBL}$ at the same position for $E_{\rm ph} = 10\,{\rm TeV}$ is due to change in the EBL spectrum at 1 eV. The average COM energies of the produced electrons are $\bar{E}_{\rm e,COM}/m_ec^2 \approx 1.5, 1.7, 2.2$, and 2.8 for $E_{\rm ph} = 0.3, 1, 3$, and 10 TeV, respectively.

in the average COM energies of the produced electrons, which are respectively, $\bar{E}_{\rm e,COM}/m_ec^2 \approx 1.5, 1.7, 2.2$ and 2.8 for $E_{\rm ph} = 0.3, 1, 3$ and 10 TeV. Hence we expect that these pairs are in the sub-relativistic to mildly-relativistic regimes in their COM frame.

4.2. *Regime of Instability*

Given that the range of $k_BT_b/m_ec^2 = E_{\rm e,COM}/m_ec^2 - 1$ falls between $0.5-2$ for $E_{\rm ph} = 1-10\,{\rm TeV}$, we now determine whether or not the reactive or kinetic instabilities apply to these beams. First, it is necessary to determine n_b/n_t. Here the target is the background IGM, so $n_t = n_{\rm IGM}$, where $n_{\rm IGM} \approx 2\times10^{-7}\,(1+\delta)\,(1+z)^3\,{\rm cm}^{-3}$ is the mean density of the IGM, z is the redshift, and δ is the overdensity. The number density of the TeV beam is more complicated as the production rate of pairs must be balanced against their loss due to plasma instabilities or ICC. This is discussed extensively in BCP12 and will not be repeated here. However, we note that the important issue here is the loss rate due to plasma instabilities, which is a nonlinear process. In BCP12, we assumed that the nonlinear loss rate was the same as the linear growth rate. This remains to be shown and is the focus of ongoing work, of which this paper lays the initial foundation.

Still some progress can be made if we use the IC rate as a lower limit to the beam cooling rate. This allows as to get an upper limit on the beam density.The ratio of the beam plasma density to the IGM, $n_b/n_{\rm IGM}$, is then (BCP12):

$$\frac{n_b}{n_{\rm IGM}} \approx \frac{L_E}{2\pi D_{\rm pp}^3 \Gamma_{\rm IC}}\frac{1}{n_{\rm IGM}} \approx 2.3\times10^{-16}\left(\frac{1+z}{2}\right)^{3\zeta-7}\left(\frac{EL_E}{10^{45}{\rm erg\,s^{-1}}}\right)\left(\frac{E}{\rm TeV}\right)\,{\rm cm}^{-3} \tag{36}$$

at the mean density of the IGM, where L_E is the isotropic luminosity per unit energy of the VHEGR source, E is the energy of the VHEGR photon, $\Gamma_{\rm IC}$ is the inverse Compton cooling rate, and the mean free path of a VHEGR

$$D_{\rm pp}(E,z) = 35\left(\frac{1+z}{2}\right)^{-\zeta}\left(\frac{E}{1\ {\rm TeV}}\right)^{-1}\ {\rm Mpc}\,, \tag{37}$$

where $\zeta = 4.5$ for $z < 1$ and $\zeta = 0$ for $z \geq 1$ (Kneiske et al. 2004; Neronov & Semikoz 2009).

In Section 3.3, we derived the controlling parameter that delineates the reactive (Equation 27) and kinetic regimes (Equation 31) by comparing the frequency spread of resonant waves, $\Delta\omega \approx k\Delta v$, with the growth rate, Γ. Applying these conditions (eqns. 27 and 31) to the ultrarelativistic $e^\pm$ pair beams of interest, we find for the controlling parameter:

$$\frac{\gamma_b^{2/3}}{\sqrt{k_BT_b/m_ec^2}}\left(\frac{n_b}{n_{\rm IGM}}\right)^{1/3} = 3.2\times10^{-2}\frac{\gamma_6^{2/3}}{\sqrt{k_BT_b/m_ec^2}} \times\left(\frac{1+z}{2}\right)^{\zeta-7/3}\left(\frac{EL_E}{10^{45}{\rm erg\,s^{-1}}}\right)^{1/3}\left(\frac{E}{\rm TeV}\right)^{1/3}, \tag{38}$$

and

$$\frac{\gamma_b}{\sqrt{k_BT_b/m_ec^2}}\left(\frac{n_b}{n_{\rm IGM}}\right)^{1/3} = 3.2\frac{\gamma_6}{\sqrt{k_BT_b/m_ec^2}} \times\left(\frac{1+z}{2}\right)^{\zeta-7/3}\left(\frac{EL_E}{10^{45}{\rm erg\,s^{-1}}}\right)^{1/3}\left(\frac{E}{\rm TeV}\right)^{1/3}, \tag{39}$$

where $\gamma_6 = \gamma/10^6$. We see from our reactive (27) and kinetic (31) conditions, that the oblique instability always exists in the kinetic regime, but the beam plasma instability is in the reactive regime for $z \gtrsim 1$, for sufficiently cold beams $k_BT_b/m_ec^2 \lesssim 0.5$, which occurs for $E_{\rm ph} \lesssim 0.3\,{\rm TeV}$, or for large γ, which occurs for $E_{\rm ph} \approx 10\,{\rm TeV}$ at $z = 0$.

In BCP12, we compared the cold plasma growth rates of the oblique and beam-plasma instabilities and noted that the oblique cold growth rate is larger. While we also noted that the oblique instability was in the kinetic regime in BCP12, which we confirmed above, we made no effort to study the regime of instability of the beam-plasma case. Here we have shown that the oblique growth rate is kinetic and the beam-plasma rate is marginally reactive. This implies that the growth rate of the beam plasma instability is similar to that of the oblique instability. In any case, we do not expect that the beam-plasma mode will have a major effect on our earlier results. First, plasma instabilities losses on the TeV pairs could easily push the beam plasma mode into the

kinetic regime by reducing n_b, but this requires a proper estimate of the effect of the nonlinear instability. This is a part of ongoing work and will be presented in a future publication. Second, while it seems that the beam plasma mode may be in the reactive regime, it is not too far from the kinetic regime, i.e., the controlling parameter, $(\gamma_b/\sqrt{k_B T_b/m_e c^2})\,(n_b/n_{\rm IGM})^{1/3}$, is order unity. Thus, both the reactive and the kinetic growth rates are similar and it likely makes little difference for the beam plasma mode which regime is assumed (in terms of growth rate). Therefore, the use of the kinetic growth rate for the oblique mode (and beam-plasma mode) in BCP12 is valid, and the results of this paper buttresses the results of Broderick et al. (2012); Chang et al. (2012); Pfrommer et al. (2012); Puchwein et al. (2012), and Lamberts et al. (2015).

5. SUMMARY AND CONCLUSION

The ultrarelativistic $e^{\pm}$ beams that result from VHEGR-EBL annihilation are subject to powerful plasma beam instabilities including the beam plasma and oblique instability. In this work, we examined these linear instabilities as they would apply to the ultrarelativistic pair beams. Our main findings are:

- We analytically calculated growth rate of the beam-plasma and oblique instabilities in both the reactive and kinetic regimes. We have recovered the reactive scalings for the beam-plasma mode $\Gamma \approx \gamma^{-1}(n_b/n_t)^{1/3}$ and the oblique mode $\Gamma \approx (n_b/\gamma n_t)^{1/3}$. In the kinetic regime, we have shown that the growth rate for both modes have the same scaling and similar normalization. Finally, we have shown that the growth rate of the kinetic oblique instability has broad support. Namely, there exists unstable modes that grow at $\approx 0.4\Gamma_0$ for any value of beam temperature and wavevector orientation for relativistic beams.
- We also delineated the regime of applicability of the kinetic and reactive calculation and found, while the kinetic growth rates are similar for both the beam plasma and oblique mode, the condition for transition between the kinetic and reactive regimes are different. In particular, the beam-plasma mode transitions at a lower value of γ in comparison to the oblique mode. This is due to a difference of $\gamma^{1/3}$ scaling between the two modes.
- We calculate the average COM energy of the ultrarelativistic pair beam using a simplified model of the spectrum of the EBL. We found that the average energy of these beams range from $E_{\rm e,COM}/m_e c^2 = 1.5 - 2.8$ for $E_{\rm ph} = 0.3 - 10\,{\rm TeV}$, with colder beams at lower energies. The average COM energies of the generated pairs implies that the oblique instability is in the kinetic regime, validating our results from BCP12.

We thank A. Bret for sharing his notes of the oblique instability and for extensive and enlightening discussions. A.E.B. and M.S. receive financial support from the Perimeter Institute for Theoretical Physics and the Natural Sciences and Engineering Research Council of Canada through a Discovery Grant. Research at Perimeter Institute is supported by the Government of Canada through Industry Canada and by the Province of Ontario through the Ministry of Research and Innovation. PC is supported by the UWM Research Growth Initiative, the NASA ATP program through NASA grant NNX13AH43G, and NSF grant AST-1255469. C.P. gratefully acknowledges support by the European Research Council under ERC-CoG grant CRAGSMAN-646955 and by the Klaus Tschira Foundation. E.P. gratefully acknowledges support by the Kavli Foundation. Support for AL was provided by an Alfred P. Sloan Research Fellowship, NASA ATP Grant NNX14AH35G, and NSF Collaborative Research Grant #1411920 and CAREER grant #1455342. GV acknowledges support from the Australian Research Council, project number DE140101960.

APPENDIX

LORENTZ FACTOR DEPENDENCE OF THE DISTRIBUTION FUNCTION AND VELOCITY DISPERSION

Here we explicitly derive the scaling of the parallel and perpendicular velocity dispersions with the Lorentz factor upon boosting the distribution function to the lab frame. Let us begin with a distribution function that is isotropic in the COM frame and depends only on energy. Therefore in the COM frame, which we denote with the subscript "COM", the distribution function is $f_{\rm COM}(E_{\rm COM}(\mathbf{x}_{\rm COM}, \mathbf{p}_{\rm COM}))$. When we move to the lab (denoted with subscript "L") frame, the integral of the distribution function remains invariant, i.e., total number, or

$$N \equiv \int f_{\rm L} d^3p_{\rm L} d^3x_{\rm L} = \int f_{\rm COM} d^3p_{\rm COM} d^3x_{\rm COM}. \tag{A1}$$

It is well-known that under Lorentz transformations (Landau & Lifshitz 1975),

$$d^3p_{\rm L} d^3x_{\rm L} = d^3p_{\rm COM} d^3x_{\rm COM}, \tag{A2}$$

so therefore,

$$f_{\rm L}[\mathbf{x}_{\rm L}(\mathbf{x}_{\rm COM}, \mathbf{p}_{\rm COM}), \mathbf{p}_{\rm L}(\mathbf{x}_{\rm COM}, \mathbf{p}_{\rm COM})] = f_{\rm COM}(E_{\rm COM}). \tag{A3}$$

Now let us consider moments of the distribution function. For clarity, it is helpful to consider moments of the

distribution function first in the COM frame. The velocity moment is:

$$\overline{\boldsymbol{\beta}}_{\rm COM} = N^{-1}\int \frac{\mathbf{p}_{\rm COM}}{\gamma_{\rm COM} m_e c} f_{\rm COM} d^3p_{\rm COM} d^3x_{\rm COM} = 0. \tag{A4}$$

We consider the lab frame to be boosted along the x-axis by β_b. More precisely, the initial inertial frame is the COM frame and the lab frame is moving with velocity $\beta_b = -|\beta_b|$ with respect to the COM frame. This gives:

$$\overline{\boldsymbol{\beta}}_{\rm L} = N^{-1}\int \frac{\mathbf{p}_{\rm L}}{\gamma_{\rm L} m_e c} f_{\rm L} d^3p_{\rm L} d^3x_{\rm L} = N^{-1}\int \frac{\mathbf{p}_{\rm L}(\mathbf{p}_{\rm COM}, \mathbf{x}_{\rm COM})}{\gamma_{\rm L}(\mathbf{p}_{\rm COM}, \mathbf{x}_{\rm COM}) m_e c} f_{\rm COM} d^3p_{\rm COM} d^3x_{\rm COM}. \tag{A5}$$

Breaking the components of $\overline{\boldsymbol{\beta}}_{\rm L}$ into components parallel and perpendicular to the boost, we find:

$$\overline{\beta}_{{\rm L},\parallel} = N^{-1}\int \frac{\beta_{{\rm COM},\parallel} + \beta_b}{1+\beta_b\beta_{{\rm COM},\parallel}} f_{\rm COM} d^3p_{\rm COM} d^3x_{\rm COM} \tag{A6}$$

$$\overline{\beta}_{{\rm L},\perp} = N^{-1}\int \frac{\beta_{{\rm COM},\perp}}{\gamma_b\left(1+\beta_b\beta_{{\rm COM},\parallel}\right)} f_{\rm COM} d^3p_{\rm COM} d^3x_{\rm COM}, \tag{A7}$$

where $\gamma_b = \left(1-\beta_b^2\right)^{-1/2}$ is the Lorentz factor of the boost between the lab and COM frame. For $|\boldsymbol{\beta}_{\mathbf{COM}}|, \beta_b \ll 1$, we recover the Galilean invariant result, $\overline{\boldsymbol{\beta}}_{\rm L} \approx \overline{\boldsymbol{\beta}}_{\rm COM} + \beta_b\hat{\boldsymbol{x}}$. However, this Galilean result no longer holds for relativistic motion.

Now we consider the dispersion around $\overline{\boldsymbol{\beta}}$. In components, the COM frame is:

$$\overline{\Delta\beta^2}_{\rm COM,i} = N^{-1}\int \beta_i^2 f_{\rm COM} d^3p_{\rm COM} d^3x_{\rm COM}. \tag{A8}$$

In the lab frame, it is again useful to break it into components – the parallel component becomes

$$\begin{aligned}\overline{\Delta\beta^2}_{{\rm L},\parallel} &= N^{-1}\int (\beta_{{\rm L},\parallel} - \overline{\beta}_{{\rm L},\parallel})^2 f_{\rm L} d^3p_{\rm L} d^3x_{\rm L} = N^{-1}\int \beta_{{\rm L},\parallel}^2 f_{\rm L} d^3p_{\rm L} d^3x_{\rm L} - \overline{\beta}_{{\rm L},\parallel}^2 \\ &= N^{-1}\int \left(\frac{\beta_{{\rm COM},\parallel}+\beta_b}{1+\beta_{{\rm COM},\parallel}\beta_b}\right)^2 f_{\rm COM} d^3p_{\rm COM} d^3x_{\rm COM} - \overline{\beta}_{{\rm L},\parallel}^2,\end{aligned} \tag{A9}$$

while the perpendicular component becomes

$$\overline{\Delta\beta^2}_{{\rm L},\perp} = N^{-1}\int \beta_{{\rm L},\perp}^2 f_{\rm L} d^3p_{\rm L} d^3x_{\rm L} = N^{-1}\gamma_b^{-2}\int \frac{\beta_{{\rm COM},\perp}^2}{\left(1+\beta_{{\rm COM},\parallel}\beta_b\right)^2} f_{\rm COM} d^3p_{\rm COM} d^3x_{\rm COM}. \tag{A10}$$

It is easier to look at the perpendicular component first. It is also more intuitive to study how velocity dispersions scale between the center of mass frame and the lab from for non-relativistic center of mass velocity dispersion. Hence, for $|\boldsymbol{\beta}_{\mathbf{COM}}| \ll 1$, Equation (A10) becomes to lowest order in $\boldsymbol{\beta}_{\mathbf{COM}}$

$$\overline{\Delta\beta^2}_{{\rm L},\perp} \approx \frac{\overline{\Delta\beta^2}_{{\rm COM},\perp}}{\gamma_b^2} \approx \frac{2k_BT_b}{\gamma_b^2 m_e c^2}. \tag{A11}$$

This simple scaling of the perpendicular velocity dispersion can be understood as a scaling with time between two frames boosted relative to each other, where the coordinates perpendicular to the boost axis remain invariant. This result is also in line with the transformation of temperature as $T \to T/\gamma$ under a boost, i.e., $mv^2 \approx kT$ – two factors of $1/\gamma$ from the perpendicular velocity dispersion is countered by one factor of γ from the mass. Let us now consider the parallel component (Equation A9) again to lowest order in $\boldsymbol{\beta}_{\mathbf{COM}}$:

$$\overline{\Delta\beta^2}_{{\rm L},\parallel} \approx \frac{\overline{\Delta\beta^2}_{{\rm COM},\parallel}}{\gamma_b^4} \approx \frac{k_BT_b}{\gamma_b^4 m_e c^2}, \tag{A12}$$

Here, the scaling of the parallel velocity dispersion can be understood as a double scaling of both time and coordinate (along the boost axis) between same two frames boosted relative to each other, giving an extra scaling of γ^{-2}. This scaling of the parallel component of the velocity dispersion has important consequences that we explore in the main part of the paper.

SOLUTION FOR THE REACTIVE REGIME

We begin with the dispersion relation (Equation (11)), which is

$$\epsilon = 1 - \sum_s \frac{m_e\omega_{p,s}^2}{k^2}\int F_s \mathbf{k}\cdot\boldsymbol{\nabla}_p \frac{1}{\omega - \mathbf{k}\cdot\mathbf{v}} d^3p = 1 - \sum_s \frac{\omega_{p,s}^2}{k^2c^2}\int F_s \frac{k^2c^2 - (\mathbf{k}\cdot\mathbf{v})^2}{\gamma(\omega-\mathbf{k}\cdot\mathbf{v})^2} d^3p = 0\,. \tag{B1}$$

We then take the limit of Equation (3) as $k_B T_t \to 0$, which yields a δ function. For the target plasma, we set $v_0 = 0$, and for a beam plasma $v_0 = v_b$[13]. This leads to Equation (12), which we reproduce below.

$$1 - \frac{\omega_{p,t}^2}{\omega^2} - \frac{\omega_{p,b}^2}{\gamma^3(\omega - k_z v_b)^2}\frac{\gamma^2 k_x^2 + k_z^2}{k_x^2 + k_z^2} = 0. \tag{B2}$$

Equation (B2) can be rewritten as

$$\left(\omega^2 - \omega_{p,t}^2\right)\left[(\omega - k_z v_b)^2 - \frac{\omega_{p,b}^2}{\gamma^3}\frac{\gamma^2 k_x^2 + k_z^2}{k_x^2 + k_z^2}\right] = \frac{\omega_{p,t}^2\omega_{p,b}^2}{\gamma^3}\frac{\gamma^2 k_x^2 + k_z^2}{k_x^2 + k_z^2}, \tag{B3}$$

where we have added a factor of $\gamma^{-3}\omega_{p,t}^2\omega_{p,b}^2(\gamma^2 k_x^2 + k_z^2)/(k_x^2 + k_z^2)$ to both sides. To solve the dispersion relation (B3), we take $\omega = \omega_{p,t} + \Delta\omega$ and expand to lowest order in $\Delta\omega$ and $\omega_{p,b}$. This gives

$$2\Delta\omega\omega_{p,t}\left(\Delta\omega + \omega_{p,t} - k_z v_b\right)^2 = \frac{\omega_{p,t}^2\omega_{p,b}^2}{\gamma^3}\frac{\gamma^2 k_x^2 + k_z^2}{k_x^2 + k_z^2}. \tag{B4}$$

For $\Delta\omega \ll \omega_{p,t} - k_z v_b$, $\Delta\omega$ is real and there is no instability. However, if $k_z = \omega_{p,t}/v_b$, we then have

$$\Delta\omega^3 = \omega_{p,t}^3\frac{\omega_{p,b}^2}{2\gamma^3\omega_{p,t}^2}\frac{\gamma^2 Z_x^2 + 1}{Z_x^2 + 1}, \tag{B5}$$

where we have multiplied the fraction on the right hand side by $(v_b/\omega_{p,t})^2/(v_b/\omega_{p,t})^2$ and $Z_x = k_x v_b/\omega_{p,t}$ is the dimensionless wavevector perpendicular to the beam direction. Equation (B5) gives three solutions for $\Delta\omega$: one real and two imaginary (one growing and one damping). The maximum growth rate is then

$$\Gamma = \frac{\sqrt{3}}{2^{4/3}}\left(\frac{n_b}{n_t}\right)^{1/3}\left(\frac{\gamma^2 Z_x^2 + 1}{Z_x^2 + 1}\right)^{1/3}\frac{\omega_{p,t}}{\gamma} \tag{B6}$$

SOLUTION FOR THE KINETIC REGIME

To find the growth rate for the kinetic regime, we begin first with the distribution function for the target plasma

$$F_t = \left(\frac{1}{2\pi m_e k_B T_t}\right)^{3/2}\exp\left(-\frac{p^2}{2m_e k_B T_t}\right). \tag{C1}$$

We assume that the target plasma is nonrelativistic with a momentum $\mathbf{p} = m_e\mathbf{v}$, and T_t is the temperature of the target background plasma. For the beam plasma, we adopt the Maxwell-Jüttner distribution (Equation 3). Inserting these into the dispersion relation (Equation 10), we find

$$1 - \frac{\omega_{p,t}^2}{k^2c^2}\int F_t\frac{k^2c^2 - (\mathbf{k}\cdot\mathbf{v})^2}{\gamma(\omega - \mathbf{k}\cdot\mathbf{v})^2}d^3p + \frac{m_e\omega_{p,b}^2}{k^2}\int\frac{\mathbf{k}\cdot\boldsymbol{\nabla}_p F_b}{\omega - \mathbf{k}\cdot\mathbf{v}}d^3p = 0, \tag{C2}$$

where we have integrated by parts only the second term, associated with the target plasma.

As the target plasma is nonrelativistic, we can take $v \ll c$ and $\gamma \to 1$. Expanding the denominator in powers of v, we find[14]

$$\int F_t\frac{k^2c^2 - (\mathbf{k}\cdot\mathbf{v})^2}{\gamma(\omega - \mathbf{k}\cdot\mathbf{v})^2}d^3p \approx k^2c^2\int F_t\left(\frac{1}{\omega^2} + \frac{2\mathbf{k}\cdot\mathbf{v}}{\omega^3} + \frac{3(\mathbf{k}\cdot\mathbf{v})^2}{\omega^4}\right)d^3p \approx \frac{k^2c^2}{\omega^2}\left(1 + 3k^2\lambda_D^2\right), \tag{C3}$$

where the second term is zero because it is odd, $\lambda_D^2 = k_B T_t/m_e\omega_p^2$ is the Debye length, and we have assumed that $k^2\lambda_D^2 \ll 1$ and $\omega \approx \omega_p$ in the last term on the RHS[15]. If we ignore the third term in the kinetic dispersion relation (18), this yields two plasma modes: an undamped plasma oscillation mode with $\omega = \omega_{p,t}$ and a longitudinal electron plasma wave, i.e., Langmuir wave, with

$$\omega \approx \omega_{p,t}\left(1 + \frac{3}{2}k^2\lambda_{D,t}^2\right). \tag{C4}$$

[13] That is, we set $F_s(\mathbf{p}) = \delta^3(\mathbf{p} - \mathbf{p}_{0s})$ where $\mathbf{p}_{0s} \equiv \gamma_0 m_e v_0\hat{\mathbf{z}}$ is the momentum associated with v_0.

[14] An alert reader will note that Lorentz factor, γ, and the second term in the numerator both contribute to the expansion in powers of v at second order. These contributions are the result of the minor deviations from the Lorentz factor of the nonrelativistic electrons and the subtle different between momentum and velocity at order v^2/c^2. These corrections correct the plasma frequency, ω_p at order v^2/c^2, but do not change the physics of the oscillations, i.e., they are independent of the wavevector. Hence, we ignore these effects while keeping the $O(v^2/c^2)$ correction that determine the Langmuir wave because these corrections depend on the wavevector.

[15] A direct solution to Equation (C3) without approximating $\omega \approx \omega_p$ will reveal waves with nontrivial growth or damping rates. These wave are not legitimate and result from the Taylor expansion of the denominator of Equation (C3). A correct treatment of Equation (C3) with the appropriate Landau contours will give the correct growing or damping behavoirs for waves with phase speeds approximately that of the electron phase speeds.

To compute the contribution from the beam term, we will reorient our coordinate system and define the z'-axis along the wavevector, $\mathbf{k}$. In this case we have the beam taking on a non-z' component, $\mathbf{v}_b = v_{bz'}\hat{\mathbf{z}}' + v_{bx'}\hat{\mathbf{x}}'$. This frame moves with a velocity, $\mathbf{v}_{\rm ph} = \omega_k/k\hat{\mathbf{z}}'$. With an eye toward computing the residue that will appear in Equation (18), we define $p_{z'} = \gamma_{z'} v_{z'} E_\perp$, $E = \gamma_{z'} E_\perp$, and $E_\perp = \sqrt{m^2 + p_\perp^2}$ is the perpendicular energy. In this case, we can rewrite the beam distribution function as

$$\begin{aligned} F_B &= \frac{m_e c^2}{4\pi\gamma_b k_B T_b K_2(m_e c^2/k_B T_b) m_e^3 c^3} \exp\left(-\frac{\gamma_b(E - v_{b,z'}p_{z'} - v_{b,x'}p_{x'})}{k_B T_b}\right) \\ &= \frac{\mu m_e^{-3} c^{-3}}{4\pi\gamma_b K_2(\mu)} \exp\left(-\frac{\gamma_b\gamma_{z'}(c^2 - v_{b,z'}v_{z'})E_\perp)}{k_B T_b c^2}\right) \exp\left(\frac{\gamma_b v_{b,x'} p_{x'}}{k_B T_b}\right), \end{aligned} \tag{C5}$$

where we define $\mu = m_e c^2/k_B T_b$. Inserting the equation into (C2) and using the results of Equation (C3), we find

$$1 - \frac{\omega_{p,t}^2}{\omega^2}\left(1 + 3k^2\lambda_D^2\right) + i\frac{\pi n_b}{n_t} m_e v_B^2 R = 0, \tag{C6}$$

which involves the integral of

$$R \equiv \int \frac{k\partial F_b/\partial p_{z'}}{\omega - k_{z'} v_{bz'}} d^3p, \tag{C7}$$

where R is the residue for $p_{z'}$ such that $v_{z'} = v_{\rm ph}$.

We can assume that $k\lambda_D \ll 1$ as the thermal velocity of the background plasma is much smaller than the speed of the ultrarelativistic beam. We then take $\omega = \omega_r + i\Gamma$, where $\omega_r = \Re(\omega)$ is the real part of ω and the growth rate $\Gamma \ll \omega_r$, to find:

$$\Gamma \approx -\omega_p \frac{\pi n_b}{2n_t} m_e v_B^2 R. \tag{C8}$$

Here two elements contribute to the pole:

$$\left.\frac{\partial}{\partial p_{z'}}(\omega - k v_{bz'})\right|_{\rm pole} = -k\left(\frac{c^2}{E} - \frac{p_{z'}^2 c^4}{E^3}\right)\Bigg|_{\rm pole} = -\frac{kc^2}{\gamma_{\rm ph}^3 E_\perp}, \tag{C9}$$

and

$$\begin{aligned} k\left.\frac{\partial F_b}{\partial p_{z'}}\right|_{\rm pole} &= -\frac{k\gamma_b}{k_B T_b}\left(\frac{p_{z'}c^2}{E} - v_{b,z'}\right) F_b\Big|_{\rm pole} \\ &= -\frac{k(v_{\rm ph} - v_{b,z'})\mu^2}{4\pi m_e^4 c^5 K_2(\mu)} \exp\left(-\frac{\gamma_b\gamma_{\rm ph}(c^2 - v_{b,z'}v_{\rm ph})E_\perp)}{k_B T_b c^2}\right) \exp\left(\frac{\gamma_b v_{b,x'}p_{x'}}{k_B T_b}\right). \end{aligned} \tag{C10}$$

Putting this all together, the residue is

$$R = \frac{\gamma_{\rm ph}^3(v_{\rm ph} - v_{b,z'})\mu^2}{4\pi K_2(\mu)} \frac{\mathcal{I}}{m_e^4 c^7} \quad \text{where} \quad \mathcal{I} \equiv \int d^2p_\perp E_\perp \exp\left(-\frac{\mathcal{G}(E_\perp - w p_x)}{k_B T_b}\right), \tag{C11}$$

$\mathcal{G} \equiv \gamma_b\gamma_{\rm ph}(1 - v_{b,z'}v_{\rm ph}/c^2)$, and $w \equiv \gamma_b v_{b,x'}/\mathcal{G} \leq 1$. This latter inequality is guaranteed as

$$\mathcal{G}E_\perp - \gamma_b v_{b,x'} p_{x'} = \gamma_b(E - v_{b,z'}p_{z'} - v_{b,x'}p_{x'})|_{v_{b,z'}=v_{\rm ph}} > 0 \tag{C12}$$

is the energy in beam frame and is therefore positive definite. Noting that the $\exp(-wp_{x'})$ term appears as a boosted distribution, we boost by w along the x'-axis, removing the anisotropic term from the exponential.

Thus, we define $p'_{x'} = \gamma_w(p_{x'} - wE_\perp/c^2)$ and $p'_{y'} = p_{y'}$ and find:

$$E_\perp = \gamma_w(E'_\perp + w p'_x) \quad \text{and} \quad dp_x dp_y = \frac{E_\perp}{E'_\perp} dp'_x dp'_y. \tag{C13}$$

Inserting this into Equation (C11), we find

$$\mathcal{I} = \int d^2p'_\perp \frac{E_\perp^2}{E'_\perp} \exp\left(-\frac{\mathcal{G}'E'_\perp}{k_B T_b}\right) = \pi\gamma_w^2 \int_0^\infty dp'^2_\perp \left(E'_\perp + \frac{w^2}{2}\frac{p'^2_\perp}{E'_\perp}\right) \exp\left(-\frac{\mathcal{G}'E'_\perp}{k_B T_b}\right), \tag{C14}$$

where $\mathcal{G}' \equiv \mathcal{G}/\gamma_w$. Note in the second line that we have used isotropy in $\mathbf{p}'_\perp$ to eliminate terms linear in $\mathbf{p}'_\perp$. Using the following integrals:

$$\int_0^\infty dx\sqrt{1+x}e^{-a\sqrt{1+x}} = \frac{2e^{-a}}{a^3}\left(a^2 + 2a + 2\right) \quad \text{and} \quad \int_0^\infty dx \frac{x}{\sqrt{1+x}} e^{-a\sqrt{1+x}} = \frac{4(a+1)}{a^3}e^{-a}, \tag{C15}$$

we find

$$\mathcal{I} = \frac{2\pi\gamma_w^2 m_e^3 c^4}{\mathcal{G}'^3\mu^3}\left[\left(\mathcal{G}'^2\mu^2 + 2\mathcal{G}'\mu + 2\right) + \frac{w^2}{2c^2}\left(2\mathcal{G}'\mu + 2\right)\right] \exp\left(-\mathcal{G}'\mu\right). \tag{C16}$$

Inserting this into (C11) yields

$$R = \frac{\gamma_{\rm ph}^3 \gamma_w^2 (v_{\rm ph} - v_{b,z'})}{2\mu \mathcal{G}'^3 K_2(\mu) c} \left[\left(\mathcal{G}'^2 \mu^2 + 2\mathcal{G}'\mu + 2 \right) + \frac{\gamma_b^2 v_{b,x'}^2}{2\mathcal{G}'^2 c^2} \left(2\mathcal{G}'\mu + 2 \right) \right] \exp\left(-\mathcal{G}'\mu \right) \tag{C17}$$

and therefore,

$$\Gamma \approx -\Gamma_0 \frac{\pi \gamma_w^2 \gamma_{\rm ph}^3 (v_{\rm ph} - v_{b,z'})}{4\gamma_b \mu^2 K_2(\mu) \mathcal{G}'^3 c} \left[\left(\mathcal{G}'^2 \mu^2 + 2\mathcal{G}'\mu + 2 \right) + \frac{\gamma_b^2 v_{b,x'}^2}{2\mathcal{G}'^2 c^2} \left(2\mathcal{G}'\mu + 2 \right) \right] \exp(-\mathcal{G}'\mu), \tag{C18}$$

where $\Gamma_0 \equiv \omega_p \gamma_b (n_b/n_t)(m_e v_B^2 / k_B T_b)$ is the typical maximum growth rate.

REFERENCES

Aharonian, F., et al. 2006, Nature, 440, 1018
Boyd, T. J. M., & Sanderson, J. J. 2003, The Physics of Plasmas, ed. Boyd, T. J. M. & Sanderson, J. J.
Bret, A., Gremillet, L., & Bénisti, D. 2010, Phys. Rev. E, 81, 036402
Broderick, A. E., Chang, P., & Pfrommer, C. 2012, ApJ, 752, 22
Broderick, A. E., Pfrommer, C., Puchwein, E., & Chang, P. 2014a, ApJ, 790, 137
Broderick, A. E., Pfrommer, C., Puchwein, E., Chang, P., & Smith, K. M. 2014b, ApJ, 796, 12
Chang, P., Broderick, A. E., & Pfrommer, C. 2012, ApJ, 752, 23
Chang, P., Broderick, A. E., Pfrommer, C., Puchwein, E., Lamberts, A., & Shalaby, M. 2014, ApJ, 797, 110
de Jager, O. C., Stecker, F. W., & Salamon, M. H. 1994, Nature, 369, 294
Dermer, C. D., Cavadini, M., Razzaque, S., Finke, J. D., Chiang, J., & Lott, B. 2011, ApJ, 733, L21
Dolag, K., Kachelriess, M., Ostapchenko, S., & Tomàs, R. 2011, ApJ, 727, L4
Gould, R. J., & Schréder, G. 1966, Physical Review Letters, 16, 252
Gould, R. J., & Schréder, G. P. 1967a, Physical Review, 155, 1408
—. 1967b, Physical Review, 155, 1404
Inoue, Y., & Totani, T. 2009, ApJ, 702, 523
Jüttner, F. 1911, Annalen der Physik, 340, 145
Kneiske, T. M., Bretz, T., Mannheim, K., & Hartmann, D. H. 2004, A&A, 413, 807
Kneiske, T. M., & Mannheim, K. 2008, A&A, 479, 41
Lamberts, A., Chang, P., Pfrommer, C., Puchwein, E., Broderick, A. E., & Shalaby, M. 2015, ApJ, 811, 19
Landau, L. D., & Lifshitz, E. M. 1975, The classical theory of fields
Lu, Z., Mo, H., Lu, Y., Katz, N., Weinberg, M. D., van den Bosch, F. C., & Yang, X. 2013, ArXiv e-prints
Madau, P., & Pozzetti, L. 2000, MNRAS, 312, L9
Melrose, D. B. 1986, Instabilities in Space and Laboratory Plasmas, ed. Melrose, D. B.
Menzler, U., & Schlickeiser, R. 2015, MNRAS, 448, 3405
Miniati, F., & Elyiv, A. 2013, ApJ, 770, 54
Narumoto, T., & Totani, T. 2006, ApJ, 643, 81
Neronov, A., & Semikoz, D. V. 2009, Phys. Rev. D, 80, 123012
Neronov, A., & Vovk, I. 2010, Science, 328, 73
Nikishov, A. I. 1962, JETP, 14, 393
Pfrommer, C., Chang, P., & Broderick, A. E. 2012, ApJ, 752, 24
Puchwein, E., Pfrommer, C., Springel, V., Broderick, A. E., & Chang, P. 2012, MNRAS, 423, 149
Salamon, M. H., & Stecker, F. W. 1998, ApJ, 493, 547
Schlickeiser, R., Elyiv, A., Ibscher, D., & Miniati, F. 2012a, ApJ, 758, 101
Schlickeiser, R., Ibscher, D., & Supsar, M. 2012b, ApJ, 758, 102
Schlickeiser, R., Krakau, S., & Supsar, M. 2013, ArXiv e-prints
Sironi, L., & Giannios, D. 2014, ApJ, 787, 49
Stecker, F. W., de Jager, O. C., & Salamon, M. H. 1992, ApJ, 390, L49
Takahashi, K., Mori, M., Ichiki, K., & Inoue, S. 2012, ApJ, 744, L7
Tavecchio, F., Ghisellini, G., Bonnoli, G., & Foschini, L. 2011, MNRAS, 414, 3566
Tavecchio, F., Ghisellini, G., Foschini, L., Bonnoli, G., Ghirlanda, G., & Coppi, P. 2010, MNRAS, 406, L70
Taylor, A. M., Vovk, I., & Neronov, A. 2011, A&A, 529, A144
Venters, T. M. 2010, ApJ, 710, 1530
Wright, T. P., & Hadley, G. R. 1975, Phys. Rev. A, 12, 686